

THE MOST IRON-DEFICIENT STARS AS THE POLLUTED POPULATION III STARS

YUTAKA KOMIYA¹, TAKUMA SUDA¹ AND MASAYUKI Y. FUJIMOTO^{2,3}*Draft version July 8, 2015*

ABSTRACT

We investigate the origin of the most iron-poor stars including SMSS J031300.36-670839.3 with $[\text{Fe}/\text{H}] < -7.52$. We compute the change of surface metallicity of stars with the accretion of interstellar matter (ISM) after their birth using the chemical evolution model within the framework of the hierarchical galaxy formation. The predicted metallicity distribution function agrees very well with that observed from extremely metal-poor stars. In particular, the lowest metallicity tail is well reproduced by the Population III stars whose surfaces are polluted with metals through ISM accretion. This suggests that the origin of iron group elements is explained by ISM accretion for the stars with $[\text{Fe}/\text{H}] \lesssim -5$. The present results give new insights into the nature of the most metal-poor stars and the search for Population III stars with pristine abundances.

Subject headings: stars: abundances – stars: Population III – early universe

1. INTRODUCTION

The most metal-poor stars are relics of stars formed in the early universe. If low-mass stars with mass $m \lesssim 0.8 M_{\odot}$ were born from the primordial gas, they would still exist as nuclear burning stars in our nearby field. It is still controversial whether there are such low-mass, metal-free stars, which we refer to as Population (Pop) III survivors in this paper. Recent simulations, however, raise the possibility that low-mass stars were formed in the pristine environment (see review by Bromm 2013).

Observationally, Pop III survivors have not yet been identified despite longstanding efforts (see Bond 1981). Thanks to large-scaled surveys in the Milky Way (MW) halo from the 1990s (Beers & Christlieb 2005, for reviews), several hundreds of stars with the metallicity of $[\text{Fe}/\text{H}] < -3$ are known to date and studied with high resolution spectroscopy (see e.g. Suda et al. 2008, 2011). Among them, six stars were found below $[\text{Fe}/\text{H}] < -4.5$ but with finite metallicity. For the most iron-poor star, SMSS J031300.36-670839.3 (Keller et al. 2014, hereafter SMSS 0313-6708), iron lines are not detected ($[\text{Fe}/\text{H}] < -7.52$, Bessell et al. 2015) while calcium abundance is determined to be $[\text{Ca}/\text{H}] = -7.26$. Two other stars have $[\text{Fe}/\text{H}] = -5.7$ (HE 1327-2326, Frebel et al. 2005) and -5.4 (HE 0107-5240, Christlieb et al. 2002), respectively. The remaining three lie between $-5 < [\text{Fe}/\text{H}] < -4.5$ (Caffau et al. 2011; Norris et al. 2007; Hansen et al. 2014). We refer to stars with $[\text{Fe}/\text{H}] \leq -5$ and $-5 < [\text{Fe}/\text{H}] \leq -4.5$ as hyper and ultra metal-poor (HMP and UMP) stars, respectively (c.f. Beers & Christlieb 2005).

In order to explain the absence of Pop III survivors, surface pollution with accreted metals from the interstellar matter (ISM) has been proposed (Yoshii 1981; Iben 1983). It is also argued for the extremely low metallicity of HMP stars (Shigeyama et al. 2003; Suda et al. 2004; Komiya et al. 2009b). We investigated

the change of surface iron abundance of Pop III survivors through ISM accretion using chemical evolution modelling within the framework of hierarchical structure formation (Komiya et al. 2009b, 2010), and demonstrated that Pop III survivors can be polluted up to $[\text{Fe}/\text{H}] \sim -5$. The discovery of the star with metallicity smaller by two orders of magnitude gives us a good reason to discuss the range of surface metallicity of polluted Pop III survivors.

In this paper, we revisit the problem of surface pollution using an updated chemical evolution model (Komiya et al. 2014). Our purpose is to explore the metallicity distribution function (MDF) at extremely low metallicity and discuss the origin of HMP/UMP stars. We focus on the iron abundance since lighter elements such as carbon and magnesium can be influenced by binary mass transfer (Suda et al. 2004; Komiya et al. 2007; Nishimura et al. 2009).

2. COMPUTATION METHOD

2.1. The Hierarchical Chemical Evolution Model

We compute the chemical evolution of the MW within the framework of the hierarchical structure formation in the Λ cold dark-matter universe to evaluate the surface pollution of Pop III survivors. The detailed description of our model is given in Komiya et al. (2014), and we review the characteristics relevant to the surface pollution below.

We build merger trees based on the extended Press-Schechter theory (Lacey & Cole 1993; Somerville & Kolatt 1999). The total mass of the MW is taken to be $2 \times 10^{12} M_{\odot}$ (Li & White 2008; Boylan-Kolchin et al. 2013). The low-mass limit of mini-halos is determined by the virialized temperature $T_{\text{vir}} = 10^3$ K (Tegmark et al. 1997; Yoshida et al. 2003).

The star formation rate is assumed to be proportional to the gas mass, M_{gas} , of mini-halos with the star formation efficiency (SFE), ϵ_{\star} , set constant. We register all the individual stars with metallicity $Z < 0.1 Z_{\odot}$. We adopt a log-normal form of the initial mass function (IMF). The typical mass, m_{md} , of EMP stars is estimated at $m_{\text{md}} = 2.5\text{--}20 M_{\odot}$, much higher than the present-day IMF, according to the statistics of carbon-enhanced stars among EMP stars, which arises through the mass trans-

¹ Research Center for the Early Universe, University of Tokyo, Bunkyo-ku, Tokyo, Japan

² Department of Cosmoscience, Hokkaido University, Sapporo, Hokkaido 060-0810, Japan

³ Department of Engineering, Hokkai-Gakuen University, Sapporo, Hokkaido 062-8605, Japan

fer from AGB stars in binary systems (Komiya et al. 2007, 2009a; Suda et al. 2013). We adopt $m_{\text{md}} = 10 M_{\odot}$ for EMP stars and $25 M_{\odot}$ for Pop III stars with the dispersion of $\sigma = 0.4$, and $\epsilon_{\star} = 10^{-11} \text{yr}^{-1}$ as fiducial values from the previous study (Komiya et al. 2010, see Table 1). One of the consequences of the high-mass IMF is that EMP and Pop III survivors mostly form as the secondary members in binary systems (Komiya et al. 2007). We take into account that the Lyman-Werner (LW) background prohibit star formation in the mini-halos with $T_{\text{vir}} < 10^4 \text{ K}$ formed later than $z = z_{\text{LW}} = 20$, although those formed earlier continue their star formation (Ricotti et al. 2002; Ahn & Shapiro 2007).

We assume a uniform mixing of SN ejecta in the mini-halos. The gas outflow from the mini-halos is computed for each SN and HII region as a function of their kinetic energy and the binding energy of the mini-halos. The conversion efficiency, η , of the SN explosion energy to kinetic energy is set at 0.1. It is considered to form a galactic wind that enriches the intergalactic medium (IGM) with metals. The evolution of the metal-enriched wind is followed by assuming the momentum conserving snow-plow shell model.

Some of the mini-halos are formed with IGM pre-enriched with metal by the galactic wind. In this study, we improve the treatment of the pre-enrichment by considering the distance between the mini-halos, while a random spatial distribution was assumed in the previous work. The m -th mini-halo is regarded as pre-enriched by a galactic wind from the n -th halo if the distance, $D_{n,m}$, between them is smaller than the radius, R_n , of the metal enriched region around the n -th halo at formation. The distance $D_{n,m}(t)$ is estimated following the formalism of the EPS theory in which the formation of a halo is described as the gravitational collapse of a spherical overdense region. Two halos are considered to “merge” when a halo is formed by gravitational collapse with the two halos incorporated. In this framework, the distance between the two halos that merge at time t_{merge} to form one halo of total mass M_{tot} may be approximated to the radius, r , of the spherical region of over-density with mass M_{tot} that collapses at t_{merge} .

2.2. Surface Pollution

We trace the change in the surface iron abundance of each star by ISM accretion. In this work, we also take into account the transfer of iron from the surface of a primary to the secondary member in the binary system through the stellar wind. The accreted metals are assumed to be mixed in the surface convection zones with $0.2 M_{\odot}$ for giants and of $0.0035 M_{\odot}$ for dwarfs (Fujimoto et al. 1995).

For the ISM accretion, we adopt the Bondi-Hoyle accretion formula

$$\dot{m} = \frac{4\pi(Gm)^2 \rho_{\text{gas}}}{(V_r^2 + c_s(T_{\text{gas}})^2)^{3/2}} \quad (1)$$

with the gas density, ρ_{gas} , the sound velocity, $c_s(T_{\text{gas}})$, as a function of the gas temperature, and the relative velocity, V_r , of the star to the ambient gas, and the stellar mass m .

We assume that gas in a mini-halo is concentrated in

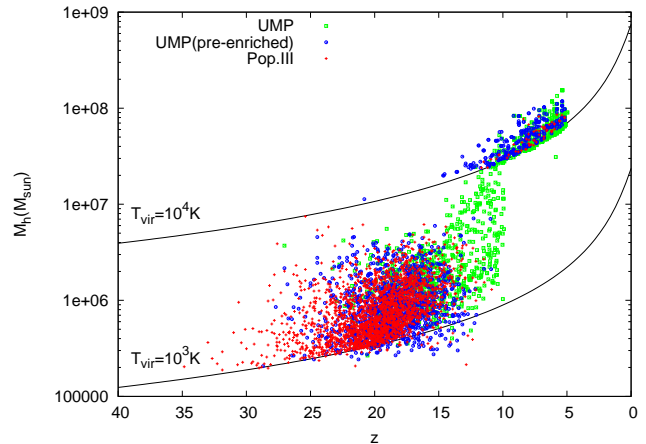


FIG. 1.— The formation redshift and the mass of host mini-halos for Pop III survivors (red crosses), the second generation UMP stars (green squares) and the first generation UMP stars in the pre-enriched mini-halos (blue circles). Lines denote the mass of mini-halos with the virial temperatures attached, its central region via isobaric contraction, i.e.,

$$\rho_{\text{gas}} = \rho_{\text{vir}}(z) \left(\frac{M_{\text{gas}}}{M_h} \right) \left(\frac{T_{\text{gas}}}{T_{\text{vir}}} \right)^{-1}, \quad (2)$$

where ρ_{vir} is the averaged density of the virialized dark-matter halos. We set $T_{\text{gas}} = 200 \text{ K}$ and 50 K for the neutral and ionized primordial clouds, respectively (Uehara & Inutsuka 2000). When the gas metallicity exceeds $[Z/H] = -6$, we change the temperature to $T_{\text{gas}} = \max(10 \text{ K}, T_{\text{CMB}}(z))$, where T_{CMB} is the temperature of the cosmic microwave background, since dust cooling becomes effective (Omukai et al. 2005; Schneider 2006).

We set $V_r = c_s$ before the host halo of the star undergoes a merger event since stars are also thought to be centrally concentrated. After the merger, stars from the smaller halo will be scattered through the merged halo with little dissipation of their kinetic energies, and we set $V_r = V_{\text{circ}}$, where V_{circ} is the circular velocity of the merged halo. The density ρ_{gas} is replaced by $\rho_{\text{vir}}(M_{\text{gas}}/M_h)$ taking into account the filling factor of gas clouds in the halo.

In the case of binary systems, the accretion rate on each member is still poorly understood. For simplicity, we take an equal accretion rate for both components, i.e., $\dot{m}_1/\dot{m}_2 = 1$, in the fiducial model.

The mass transfer rate in the binary systems is computed as a function of stellar mass and binary period with a given wind velocity from the Bondi-Hoyle formulae as in Komiya et al. (2009a).

3. RESULTS

Figure 1 shows the formation redshift and host halo mass of Pop III and UMP survivors for the model with the fiducial parameters given in Table 1. In this model, 2100–2500 low-mass Pop III stars are formed in mini-halos with $\sim 10^6 M_{\odot}$ around $z \simeq 20$. Most of the second generation stars have metallicity of $[\text{Fe}/\text{H}] > -4$ since the iron from one SN of $\sim 0.07 M_{\odot}$ is mixed with the gas of $\sim 10^5 M_{\odot}$. After $z = z_{\text{LW}} = 20$, newly formed mini-halos are prevented from forming stars by the LW radiation, while those formed at earlier epochs, two thirds of which are still metal-free, continue to form stars. The mini-halos later formed grow in mass to have $T_{\text{vir}} > 10^4 \text{ K}$

TABLE 1
PARAMETERS AND THEIR FIDUCIAL VALUE

parameter	description	fiducial value
ϵ_*	star formation efficiency	10^{-11} yr^{-1}
$m_{\text{md,emp}}$	median mass of IMF for EMP stars	$10 M_\odot$
$m_{\text{md,p3}}$	median mass of IMF for Pop III stars	$25 M_\odot$
σ	variance of IMF	0.4
η	kinetic energy fraction for SNe	0.1
z_{LW}	redshift of Lyman-Werner radiation	20
f_b	binary fraction	0.5
$n(q)$	mass ratio distribution of binaries	1
\dot{m}_1/\dot{m}_2	ratio of ISM accretion rate on each binary component	1

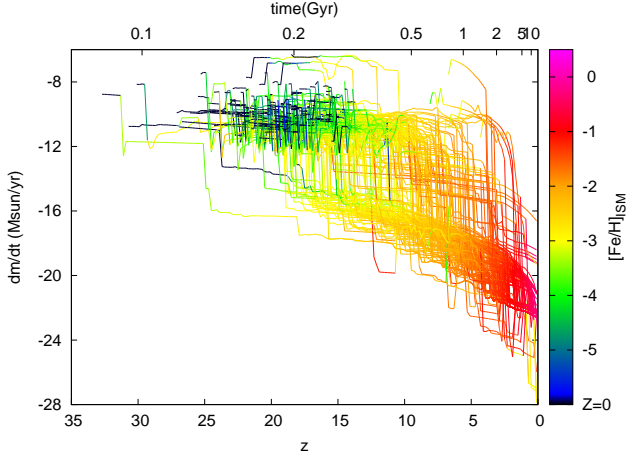


FIG. 2.— Variations of the ISM accretion rate for the sampled Pop III survivors plotted against the redshift. The metallicity of accreting gas is color-coded.

by $z \lesssim 10$ and form ~ 100 Pop III survivors. The second generation stars in these massive halos have lower metallicity of $-5 \lesssim [\text{Fe}/\text{H}] \lesssim -4$ because SN ejecta is mixed homogeneously with a larger mass of gas. The first generation of stars in mini-halos with pre-enriched IGM have metallicity around $-6 \lesssim [\text{Fe}/\text{H}] \lesssim -2$. They account for half of the UMP stars.

Figure 2 illustrates the ISM accretion rate with the metallicity of accreting gas color-coded as a function of the redshift for the sampled Pop III survivors. The accretion rate is much higher in the host mini-halos than in the merged halos because V_r increases after a merger event. Typically Pop III survivors accrete $\sim 10^{-8.5} M_\odot$ of iron to have the surface metallicity of $[\text{Fe}/\text{H}] \sim -5$ for giant stars, and $[\text{Fe}/\text{H}] \sim -3$ for dwarfs. The surface metallicity of Pop III survivors spans a wide range between $-8 \lesssim [\text{Fe}/\text{H}] \lesssim -2$ depending on the merging history of host halos and the mass of the primary stars of Pop III survivors. The abundance pattern of the polluted Pop III stars should be similar to those of EMP stars because accretion in the early universe with $[\text{Fe}/\text{H}] \lesssim -3$ is more efficient than metal-rich counterparts.

Figure 3 shows the predicted MDFs for the polluted Pop III and EMP stars, and the observed samples taken from the SAGA database (Suda et al. 2008, 2011) and from the Hamburg/ESO (HES) survey (Schöerck et al. 2009). The SAGA data has more accurate metallicity than Schöerck et al. (2009) due to higher resolution, though biased toward lower metallicity of $[\text{Fe}/\text{H}] \lesssim -3$.

In our previous study, we computed the MDF without the effects of LW feedback and SN-driven gas out-

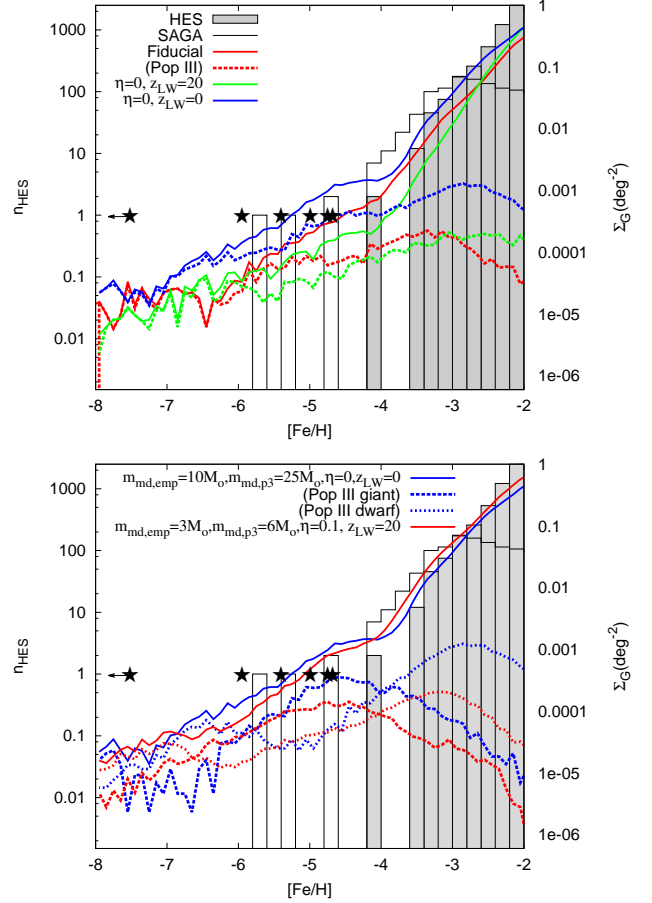


FIG. 3.— The predicted metallicity distribution functions (MDFs) compared with the observations (histograms). Star symbols denote the abundances with 3D corrections for stars with $[\text{Fe}/\text{H}] < -4.5$. Left and right axes represent the observed number and surface number density of stars, respectively. *Top panel:* The predicted MDFs of all stars (solid line) and the polluted Pop III stars (dashed line) for the fiducial model (red) and models without SN-driven outflow (green) and without SN-driven outflow and Lyman-Werner feedback (blue). *Bottom panel:* The same as the top panel but for the intermediate-mass IMF model with the feedback and the de Vaucouleurs profile (red) and the high-mass IMF model without the feedback effects (blue). Dashes and dotted lines denote the MDFs of Pop III giants and dwarfs, respectively. See text for details.

flow (Komiya et al. 2010). The top panel shows the dependences on these feedback effects. The LW feedback decreases the number of stars by prohibiting star formation in small mini-halos without metals. SN-driven gas outflow also decreases the number at $[\text{Fe}/\text{H}] > -2.5$ because it reduces the mass of star forming gas. For $[\text{Fe}/\text{H}] < -2.5$, however, the number of stars rather

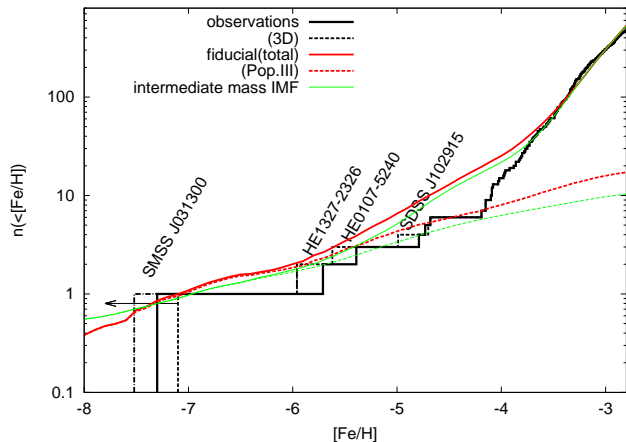


FIG. 4.— The cumulative MDF of all stars (solid line) and polluted Pop III stars (dashed line) for the fiducial model (red) and the intermediate-mass IMF model (green). Histograms represent the cumulative numbers of observed stars taken from the SAGA database and from Keller et al. (2014) and Hansen et al. (2014). Dashed line is based on the abundances with 3D corrections, and dash-dotted line is the 3D non-LTE abundance by Bessell et al. (2015). The model results are scaled to match the observations at $[\text{Fe}/\text{H}] = -3$.

swells as a result of pre-enrichment. In addition, in the $\eta = 0$ model, a majority of dwarf EMP stars becomes $[\text{Fe}/\text{H}] > -3$ due to efficient surface pollution.

We compare the absolute number of stars predicted with the HES data considering its survey area and selection efficiency. The fiducial model predicts a smaller number of EMP survivors, while the model without the feedbacks gives the number in agreement with observations when we assume a homogeneous surface density of EMP halo stars. Additionally, if we adopt the de Vaucouleur density profile for the stellar halo, the scaling factor can be smaller by a factor of five. It is to be noted, however, that the number of EMP survivors is determined by the production ratio of low- to high-mass stars since the latter dominates the chemical evolution. In our models, it depends on the m_{md} and σ of the IMF, the binary fraction f_b , and the MRD. For example, we present the result with the intermediate-mass IMF, $m_{\text{md,emp}} = 3 M_{\odot}$ and $m_{\text{md,p3}} = 5 M_{\odot}$, in the bottom panel. This model results in the number of survivors larger by 0.7 dex, compatible with the observation under the de Vaucouleur density profile. The shape of the MDF has little dependence on the adopted IMF. In all cases, stars with $[\text{Fe}/\text{H}] < -5$ are polluted Pop III stars except for a small contribution from the first generation stars in pre-enriched halos.

Figure 4 shows the cumulative MDFs. The observed data are taken from the SAGA sample, and added from Keller et al. (2014); Hansen et al. (2014) and Bessell et al. (2015) to complete the HMP/UMP sample. We also show the abundances with 3D corrections when available. The broad distribution of polluted Pop III survivors agrees with the distribution of the observed stars at the lowest metallicity range. The metallicity range of the HMP stars including SMSS 0313-6708 is covered by the polluted Pop III survivors. We estimate the iron abundance of SMSS 0313-6708 to be around $[\text{Fe}/\text{H}] \simeq -7.58$ from the observed calcium abundance ($[\text{Ca}/\text{H}] = -7.26$) and the typical enhancement of calcium for EMP stars ($[\text{Ca}/\text{Fe}] \simeq +0.32$). The iron abun-

dance is unlikely to be $[\text{Fe}/\text{H}] < -8.0$ in our scenario because 98% of EMP stars show $[\text{Ca}/\text{Fe}] < +0.74$. Note that the expected number of observed stars is ~ 1 at $[\text{Fe}/\text{H}] < -7.0$, ~ 0.6 at $[\text{Fe}/\text{H}] < -7.6$, and ~ 0.4 at $[\text{Fe}/\text{H}] < -8.0$. We see a slight overabundance for the model results around $[\text{Fe}/\text{H}] \simeq -5$ to -4 . This is an artifact resulting from the assumption of homogeneous mixing of SN ejecta in such massive halos as $M_h > 10^7 M_{\odot}$, and can be alleviated by considering possible inhomogeneous mixing.

We also check the dependencies on other model parameters. There are minor corrections to the fiducial model by changing m_1/m_2 . Binary parameters such as f_b and $n(q)$ affect the number of Pop III and EMP survivors but have little effect on the metallicity distribution. On the other hand, the MDF at the lowest metallicity is affected by the SFE; we find a rapid decline at $[\text{Fe}/\text{H}] \lesssim -6$ for $\epsilon_{\star} = 10^{-10} \text{yr}^{-1}$, because of the higher metallicity that the ISM reached before the merger events.

4. CONCLUSIONS AND DISCUSSION

We have explored the change in the surface iron abundance of low-mass survivors of Pop III stars by the accretion of ISM using the chemical evolution model within the framework of hierarchical structure formation.

Our model can reproduce the MDF observed for Galactic halo stars with $[\text{Fe}/\text{H}] < -2.5$. The MDF of polluted Pop III giants peaks around $[\text{Fe}/\text{H}] \simeq -5$ and extends to cover the whole metallicity range of HMP stars including SMSS 0313-6708. A wide spread of metallicity of polluted Pop III stars arises from the intervals from the birth to the merger of host halos and the mass of primary stars. The results little depend on the adopted IMF, and the binary parameters, but are dependent on the SFE.

Surface pollution is most effective in the mini-halos of small mass because the Bondi-Hoyle accretion rate is strongly dependent on the relative velocity of stars to the ambient gas (e.g., Suda et al. 2004; Komiya et al. 2009a). This explains the difference from Frebel et al. (2009), who considered only the surface pollution during passage through the MW disk. Johnson & Khochfar (2011) argued the suppression of ISM accretion by alleged solar-like winds from Pop III survivors. However, little is known about the mass loss from Pop III stars with a complete lack of metals and also in the possible absence of magnetic fields. In addition, their argument on the dynamics of Pop III survivors in the mini-halos may not be relevant for those belonging to binaries with more massive stars. We note that Hattori et al. (2014) report possible observational evidence for the surface metal pollution, finding that the median metallicity of halo G-type dwarfs may be systematically higher than that of K-type dwarfs with the same kinematics.

The present results indicate that such small abundances of iron group elements as observed from HMP stars are readily explained in terms of the ISM accretion. It is true that HMP/UMP stars show various peculiar abundance patterns other than the large enhancement of carbon, i.e., the enhancement of N, O, and light elements (Na, Mg, and Al), and also of Sr. These elements can be synthesized and brought to the surface in low- and intermediate-mass stars during the AGB phase (Nishimura et al. 2009; Yamada et al. 2015), and

transferred onto their low-mass secondary companions (Suda et al. 2004; Komiya et al. 2007). We will discuss the relevance of the nucleosynthesis and material mixing in AGB stars to the observed abundance patterns in a subsequent paper (Suda et al. 2015).

As an alternative scenario for the origin of HMP stars, it has been argued that they are the stars formed from the matter polluted with the ejecta from “faint SNe” with large C/Fe ratios (e.g. Umeda & Nomoto 2003; Iwamoto et al. 2005). Keller et al. (2014); Ishigaki (2014); Marassi et al. (2014), and Bessell et al. (2015) argue that the abundance pattern of SMSS 0313-6708 is consistent with the ejecta of a peculiar SN with small (or no) iron ejection. However, this scenario demands manipulation of reducing the ejection of iron by many orders of magnitude ($\sim 10^4$ -th or less). It must be noted that large C/Fe ratio results solely from the reduction of iron ejecta in “faint SNe” since the amount of carbon produced hardly differ from ordinary SNe. There should be an account for producing such large carbon abundances and variations as $[C/H] = -1.3 - -2.4$ ob-

served for HMP stars with almost similar amount of carbon ejected (Suda et al. 2004; Komiya et al. 2007).

In recent simulations of first star formation, low-mass stars can be formed at the same sites as massive stars (e.g. Clark et al. 2008; Greif et al. 2011; Smith et al. 2011; Dopcke et al. 2013; Stacy & Bromm 2014). This opens a new path for low-mass Pop III star formation in addition to ionized primordial gas in the mini-halos with $T_{\text{vir}} \gtrsim 10^4$ K (Uehara & Inutsuka 2000). Our scenario indicates that Pop III survivors, found in the Milky Way halo, should have suffered more or less from surface pollution by the ISM accretion. In order to confirm the formation of Pop III low-mass stars, therefore, we have to seek for un-polluted Pop III survivors, which are expected to have been expelled from the host halos. We will discuss the search for these pristine Pop III stars in a forthcoming paper.

This work is partially supported by Grant-in-Aid for Scientific Research (23224004, 25400233, 25800115).

REFERENCES

- Ahn, K., & Shapiro, P. R. 2007, *MNRAS*, 375, 881
 Beers, T. C., & Christlieb, N. 2005, *ARA&A*, 43, 531
 Bessell, M. et al. 2015, arXiv:1505.03756
 Bond, H. E. 1981, *ApJ*, 248, 606
 Boylan-Kolchin, M., Bullock, J. S., Sohn, S. T., Besla, G., van der Marel, R. P. 2013 *ApJ*, 768, 140
 Bromm, V. 2013, *RPPH*, 76, 2901
 Caffau, E., et al. 2011, *Nature*, 477, 67
 Christlieb, N., Bessell, M. S., Beers, T. C., Gustafsson, B., Korn, A., Barklem, P. S., Karlsson, T., Mizuno-Wiedner, & M., Rossi, S. 2002, *Nature*, 419, 904
 Clark, P. C., Glover, S. C. O., & Klessen, R. S. 2008, *ApJ*, 672, 757
 Dopcke, G., Glover, S. C. O., Clark, P. C., & Klessen, R. S. 2013, *ApJ*, 766, 103
 Frebel, A., et al. 2005, *Nature*, 434, 871
 Frebel, A., Johnson, J. L., & Bromm, V. 2009, *MNRAS*, 392, 50
 Fujimoto, M. Y., Sugiyama, K., Iben, I. Jr., & Hollowell, D., 1995, *ApJ*, 444, 175
 Greif, T. H., Springel, V., White, S. D. M., Glover, S. C. O., Clark, P. C., Smith, R. J., Klessen, R. S., & Bromm, V. 2011, *ApJ*, 737, 75
 Hansen, T. et al. 2014, *ApJ*, 787, 162
 Hattori, K., Yoshii, Y., Beers, T. C., Carollo, D., & Lee, Y. S. 2014, *ApJ*, 784, 153
 Iben, I. Jr., 1983, *Mem. S. A. It.*, 54, 321
 Ishigaki, M. N., Tominaga, N., Kobayashi, C., & Nomoto, K. 2014, *ApJ*, 792, L32
 Iwamoto, N., Umeda, H., Tominaga, N., Nomoto, K., & Maeda, K. 2005, *Science*, 309, 451
 Johnson, J. L., & Khochfar, S. 2011, *MNRAS*, 413, 1184
 Keller, S. C., et al. 2014, *Nature*, 506, 463
 Komiya, Y., Habe, A., Suda, T., & Fujimoto, Y. M. 2009, *ApJ*, 696, L79
 Komiya, Y., Habe, A., Suda, T., & Fujimoto, Y. M. 2010, *ApJ*, 717, 542
 Komiya, Y., Suda, T., & Fujimoto, Y. M. 2009, *ApJ*, 694, 1577
 Komiya, Y., Suda, T., Minaguchi, H., Shigeyama, T., Aoki, W., & Fujimoto, Y. M. 2007, *ApJ*, 658, 367
 Komiya, Y., Yamada, S., Suda, T., & Fujimoto, Y. M. 2014, *ApJ*, 783, 132
 Lacey, C., & Cole, S. 1993, *MNRAS*, 262, 627
 Li, Y.-S., & White, S. 2008, *MNRAS*, 384, 1459
 Marassi, S., Chiaki, G., Schneider, R., Limongi, M., Omukai, K., Nozawa, T., Chieffi, A., & Yoshida, N. 2014, *ApJ*, 794, 100
 Nishimura, T., Suda, T., Aikawa, M. et al. 2008, *PASJ*, 61, 909
 Norris, J. E., Christlieb, N., Korn, A. J., Eriksson, K., Bessell, M. S., Beers, T. C., Wisotzki, L., and Reimers, D. 2007, *ApJ*, 670, 774
 Omukai, K., Thuribe, T., Schnerder, R., & Ferrara, A., 2005, *ApJ*, 626, 627
 Ricotti, M., Gned, N. Y., & Shull, J. M. 2002, *ApJ*, 575, 49
 Schneider, R., Omukai, K., Inoue, A. K., & Ferrara, A. 2006, *MNRAS*, 369, 1437
 Schöerck, T., Christlieb, N., et al. 2009, *A&A*, 507, 817
 Shigeyama, T., Tsujimoto, T., & Yoshii, Y. 2003, *ApJ*, 586, L57
 Smith, R. J., Glover, S. C. O., Clark, P. C., Greif, T., & Klessen, R. S. 2011, *MNRAS*, 414, 3633
 Somerville, R. S., & Kolatt, T. S. 1999, *MNRAS*, 305, 1
 Stacy, A., & Bromm, V. 2014, *ApJ*, 785, 73
 Suda, T., Aikawa, M., Machida, Fujimoto, M. Y., Iben, I. Jr. 2004, *ApJ*, 611, 476
 Suda, T., et al. 2008, *PASJ*, 60, 1159
 Suda, T., et al. 2011, *MNRAS*, 412, 843
 Suda, T., et al. 2013, *MNRAS*, 432, L46
 Suda, T., et al. 2015, in prep.
 Tegmark, M., Silk, J., Rees, Blanchard, A., Abel, T., & Palla, F. 1997, *ApJ*, 474, 1
 Uehara, H., & Inutsuka, S.-i. 2000, *ApJ*, 531, L91
 Umeda, H., & Nomoto, K. 2003, *Nature*, 422, 871
 Yamada, S., Suda, T., Komiya, Y., & Fujimoto, M.-Y. 2015, in prep.
 Yoshida, N., Abel, T., Hernquist, L., Sugiyama, N. 2003, *ApJ*, 592, 645
 Yoshii, Y. 1981, *A&A*, 97, 280